Persistence of the Jahn–Teller distortion of Mo^{5+} in double perovskites: a structural study of Ba_2NdMoO_6 and the effect of chemical doping in $Ba_2Nd_{1-x}Y_xMoO_6$†‡

Edmund J. Cussen* and William J. Cameron

Received 26th August 2009, Accepted 20th November 2009
First published as an Advance Article on the web 11th December 2009
DOI: 10.1039/b917579b

The cation-ordered perovskites Ba_2NdMoO_6 and $Ba_2Nd_{1-x}Y_xMoO_6$ have been structurally characterised by a combination of neutron and X-ray powder diffraction. Ba_2NdMoO_6 retains the tetragonal room temperature structure on cooling to 150 K [$I4/m$; $a = 5.98555(5)$ Å, $c = 8.59510(10)$ Å] although the MoO_6 octahedra distort with an elongation of two *trans* Mo–O bonds. Neutron diffraction data collected at $T \leq 130$ K show that this compound has undergone a structural distortion to a triclinic space group, although the MoO_6 octahedra do not distort any further on cooling below this temperature [at 130 K: $I\bar{1}$; 5.97625(14) Å, 5.9804(2) Å, 8.59650(13) Å, 89.876(2)°, 89.921(3)°, 89.994(2)°]. The room temperature tetragonal space group symmetry of Ba_2NdMoO_6 is preserved in the series $Ba_2Nd_{1-x}Y_xMoO_6$ up to composition $0.35 \leq x < 0.5$. The lattice parameters converge as the value of x increases until cubic symmetry is reached for the composition of $Ba_2Nd_{0.5}Y_{0.5}MoO_6$ [$Fm\bar{3}m$; $a = 8.4529(3)$ Å]. Magnetic susceptibility measurements show that all of these compounds display the Curie–Weiss behaviour associated with a fully localised electronic system. The paramagnetic moments show good agreement with those anticipated to arise from the spin-only contribution from Mo^{5+} ($S = 1/2$, $\mu_{so} = 1.73\ \mu_B$) and the moment of $3.62\ \mu_B$ associated with the spin–orbit coupling of the $^4I_{9/2}$ ground state of Nd^{3+}. For $x \leq 0.125$ this series shows a magnetic transition in the range 10 to 15 K indicative of a distortion of the MoO_6 octahedra in these compounds that is similar to Ba_2NdMoO_6.

Introduction

The perovskite is arguably the most intensely studied structure due to the extensive range of stoichiometries that can be found within this family of compounds.[1] This structural versatility is due to the wide range of adjustments and distortions that can occur to allow substantial deviations from the prototypical structure to be accommodated. The simplest perovskite contains a large cation, such as Sr^{2+}, in the centre of a primitive cubic cell coordinated to 12 anions, commonly oxide, that are found half way along every cell edge. The corners of the cube are occupied by a smaller cation, such as Ti^{4+}, that is octahedrally coordinated by six anions. By considering the ions as hard spheres in contact with one another it is possible to describe the ideal ratio of cation and anion sizes and use a tolerance factor to empirically describe departures from this situation.[2] The ubiquitous nature of perovskites arises from the ability of the structure to distort from the primitive cubic model described above in an astonishing number of ways: by rotation of the oxide octahedra around one, two or three axes; by these rotations being in the same sense or alternating phase in adjacent octahedra;[3] by distortion of the octahedra;[4] by displacement of the cations due to sterically active lone pair or other electronic effects;[4] or combinations of these effects. When one considers additional complicating factors, such as charge ordering in mixed oxidation state compounds,[5] chemical ordering when more than one cation can occupy either the twelve[6] or six-coordinate sites,[7,8] possible anion deficiency[9] and vacancy ordering,[10,11] it can be seen that there is scope for an unrivalled diversity in the chemistry of this apparently simple structure.

This structural flexibility provides a unique playground both to test how electronic behaviour is affected by adjusting the structure and to deliberately manipulate the structure in order to induce exotic and/or useful behaviour such as magnetoresistance,[12] ionic conduction[13] or multiferroic behaviour.[14] There is considerable interest in the behaviour of perovskites containing a mixture of cations in the octahedrally coordinated sites as this can allow an additional degree of freedom in manipulating the magnetic exchange interactions.[7,15] If these two cations are sufficiently different in either size or charge then the increase in the lattice strain or electrostatic charge that arises from having like cations in adjacent octahedra is sufficiently large to overcome entropic considerations and drive the structure towards an ordered array of cations.[16] In the case of two cations present in equal concentration this almost always leads to a rock salt arrangement of cations to give a face-centred cubic structure. The cations on such a lattice form a series of equilateral triangles. If the super-exchange interactions between these cations are antiferromagnetic then the interactions around each triangle are perfectly cancelled and it is not possible for a collinear, non-degenerate magnetic ground state to be formed.[17]

WestCHEM, Department of Pure and Applied Chemistry, The University of Strathclyde, Thomas Graham Building, 295 Cathedral Street, Glasgow, G1 1XL, UK. E-mail: Edmund.Cussen@Strath.ac.uk

† Electronic supplementary information (ESI) available: Additional magnetic susceptibility data for all compositions. See DOI: 10.1039/b917579b

‡ This paper is part of a *Journal of Materials Chemistry* issue highlighting the work of emerging investigators in materials chemistry.

Previous studies of Ba_2LnMoO_6 have found that for all but the largest lanthanides these compounds form face-centred cubic perovskites.[18,19] These phases contain a fully ordered arrangement of Ln^{3+} and Mo^{5+} that requires a doubling of the unit cell lengths compared to the lattice parameter of a simple cubic perovskite, $a_p \approx 4.2$ Å. In all of these compounds the $S = 1/2$ spin of Mo^{5+} displays localised paramagnetic behaviour to the lowest measured temperatures, 2 K, due to perfect magnetic frustration resulting from the cancellation of the antiferromagnetic interactions that could otherwise be expected to lead to antiferromagnetic ordering at temperatures $50 < T/K < 100$.[19] By replacing the 12-coordinate Ba^{2+} cation with the smaller Sr^{2+} species it is possible to induce distortions from cubic symmetry that lift the degeneracy of the magnetic interactions and allow an ordered magnetic ground state to develop. However, even in the case of gross departures from the ideal structure the magnetic ordering temperature in Sr_2ErMoO_6 was no higher than 4 K.[20]

The behaviour of the compound Ba_2NdMoO_6 is exceptional.[19] This phase displays a small distortion at room temperature to adopt the tetragonal space group *I*4/*m* that can be understood in geometric terms as necessary to satisfy the bonding requirements of the Ba^{2+} cation. Where this compound differs from other A_2LnMoO_6 is the behaviour at low temperature. $Ba_{1.5}Sr_{0.5}ErMoO_6$ and $Ba_{1.2}Sr_{0.8}ErMoO_6$ share the *I*4/*m* room temperature structure and remain paramagnetic to 2 K as would be expected due to substantial magnetic frustration arising from the minimal departure from the perfect frustration associated with cubic symmetry.[20] However, Ba_2NdMoO_6 undergoes a transition at 15 K to form an antiferromagnetically ordered phase. We have previously shown that the anisotropic coupling manifested in this magnetic structure is related to a structural distortion of the MoO_6 octahedra that is evident at low temperature. This distortion involves an elongation of two of the Mo–O bonds and partially lifts the degeneracy of the t_{2g} orbitals and confers stability on the d_{xz} and d_{yz} orbitals, which remain pseudo-degenerate, at the expense of destabilising the d_{xy} orbital. As Mo^{5+} has a single electron it is unclear why the opposite distortion, involving contraction of two Mo–O bonds, does not occur instead and provide double the electronic stabilisation energy. Nevertheless, the clear driver for this distortion comes from electronic stabilisation from partial lifting of degeneracy and so this has been identified as a Jahn–Teller distortion driven by Mo^{5+}.

The low temperature structure of Ba_2NdMoO_6 (Fig. 1) identified a change in space group symmetry from that observed at room temperature to the centrosymmetric triclinic space group described in a non-standard setting $I\bar{1}$ that uses the same unit cell setting as the tetragonal space group. The relationship between the distortions of the MoO_6 octahedra driven by the electronic instability of Mo^{5+} in a regular octahedron and the phase change from *I*4/*m* to $I\bar{1}$ is unclear.

A detailed study of the temperature dependence of the structure of Ba_2SmMoO_6 has revealed some similar behaviour in this compound.[21] At elevated temperatures Ba_2SmMoO_6 adopts a tetragonally distorted structure as observed for Ba_2NdMoO_6 at room temperature. However, on cooling to 353 K Ba_2SmMoO_6 undergoes a structural transition to the same triclinic space group, $I\bar{1}$, as observed for Ba_2NdMoO_6 at $T \leq 32$ K. In Ba_2SmMoO_6 a Jahn–Teller distortion occurs simultaneously with the onset of an antiferromagnetically ordered state at $T_N =$ 130 K. This is an order of magnitude greater than the antiferromagnetic ordering temperature of Ba_2NdMoO_6 and simultaneous occurrence of structural distortion and magnetic ordering suggests that the orbital ordering manifested by the distortion of the MoO_6 octahedra precipitates the antiferromagnetic order. These two compounds are the only example of Jahn–Teller distortions involving Mo^{5+}. Considering the near ubiquitous nature of electron degeneracy in the t_{2g} orbitals amongst early transition metal cations of the 4d and 5d series it is possible that these are the first examples of a more wide spread phenomena. The strong coupling between electronic and structural properties and the surprisingly high magnetic ordering temperature indicated in Ba_2SmMoO_6 suggest that this behaviour of Mo^{5+} may provide a new tool for manipulating electronic properties of oxides.

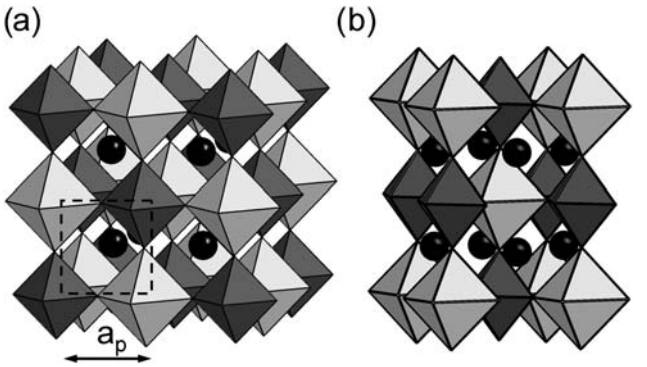

Fig. 1 (a) The face-centred cubic structure of Ba_2YMoO_6 and (b) the triclinic structure of Ba_2NdMoO_6 at 3.5 K. Black spheres represent Ba^{2+} cations and dark and light grey octahedra represent MoO_6 and LnO_6 units respectively. The unit cell and lattice parameter, a_p, of the primitive cubic perovskite subcell are indicated in (a).

Here we describe experiments designed to probe further the behaviour of Ba_2NdMoO_6. We have used variable temperature neutron diffraction to examine the structural evolution between the tetragonal phase with regular MoO_6 octahedra observed at room temperature and the triclinic Jahn–Teller distorted phase identified around the magnetic transition temperature of 15 K. We also report preliminary structural and magnetic properties of a series of compounds $Ba_2Nd_{1-x}Y_xMoO_6$ that show for the first time that the anomalous magnetic transitions observed in Ba_2SmMoO_6 and Ba_2NdMoO_6 can survive structural manipulation through chemical doping.

Experimental

Polycrystalline samples were prepared from stoichiometric mixtures of barium carbonate, molybdenum trioxide, neodymium oxide and yttrium oxide as appropriate. Nd_2O_3 and Y_2O_3 were stored at 800 °C in order to prevent uptake of carbon dioxide. These mixtures were ground thoroughly and pressed into pellets before being heated in air from 500 °C to 800 °C at 1 °C min^{-1}. This initial heating was necessary to prevent the loss of molybdenum from the reaction mixture that occurs if the unreacted mixture sample is placed directly into a furnace at 800 °C. The samples were then heated at temperatures up to 1350 °C under a flowing atmosphere of 5% H_2 in N_2. In every

case the sample was cooled to room temperature under this atmosphere. The progress of the reactions was followed using X-ray powder diffraction. After repeated regrinding and repressing of the reaction mixtures and repeatedly heating the samples over several days, the diffraction pattern could be completely indexed using a unit cell indicative of a cation-ordered perovskite and so indicated that the reaction was complete.

X-Ray powder diffraction data were collected using a Siemens D500 diffractometer operating in Bragg Brentano geometry using Cu Kα radiation. Data suitable for Rietveld analysis were collected over the range $8 \leq 2\theta/^\circ \leq 100$ with a step size of $2\theta = 0.02^\circ$. Neutron powder diffraction data were collected using the high resolution instrument D2B at the Institut Laue Langevin in Grenoble. Diffraction data were analysed using the Rietveld method[22] of structure refinement as implemented in the GSAS suite of programs.[23] A shifted Chebyshev function was used to fit the background empirically and a pseudo Voigt function modelled the peak shape.

Magnetic susceptibility measurements were conducted using a MPMS SQUID magnetometer using *ca.* 70 mg of sample contained in a gelatin capsule. Data were collected after cooling the sample in zero applied field (zfc) and in the applied field (fc) of 100 G.

Results

Neutron diffraction data collected from Ba_2NdMoO_6 at 150 K and 190 K could be satisfactorily indexed using the tetragonal space group *I*4/*m* that we have previously observed for this compound at room temperature. It should be noted that the triclinic distortion seen for this compound at low temperature shares the same systematic absences as the higher temperature phase and so discrimination between the room temperature tetragonal phase and the low temperature triclinic phase requires careful examination of the intensity distribution in the peaks in the neutron diffraction profile. The peaks at higher angle provide the clearest indication of the symmetry of the structure and, as can be seen in Fig. 2, the neutron diffraction profile can be satisfactorily modelled using the single reflections imposed by the symmetry constraints of the *I*4/*m* space group. Data collected at 130 K clearly show splitting in the high angle peaks that is incompatible with the tetragonal space group. However, this complex intensity distribution could readily be modelled using the triclinic $I\bar{1}$ symmetry previously observed for this phase at temperatures below 32 K.

Trial refinements against these data showed that there is no detectable disorder in the Nd^{3+}/Mo^{5+} distribution over the different sites and that the oxide positions are fully occupied. Both of these observations have been made consistently for multiple compounds from the series Ba_2LnMoO_6 and $Ba_{2-x}Sr_xErMoO_6$.[18–20] Refinement of the displacement parameters led to extremely small negative values for the metal cations that were within 5 standard deviations of zero. A negative value for a displacement has no physical meaning. However, Rietveld refinement typically underestimates the standard deviation in refined parameters, as indicated by the Debye–Watson d-statistic[24] that for all of these refinements is *ca.* 1.0 compared to a confidence limit of around 1.9. Consequently these negative values do not represent a significant departure from zero. The origins of these values are unclear. The same compound has been studied at 3.5 K using the same diffractometer and the refinements against these data yielded physically reasonable values. Refinement of an absorption parameter failed to provide a correction to the values obtained in the present study. A trial refinement was performed against the data collected at 80 K in which the displacement parameters were fixed at positive values of the same magnitude as the negative refined values. This had no significant effect on any of the other variables in the refinement and all interatomic distances remained within one standard deviation of the values obtained when refined displacement parameters were allowed to take negative values. Fixing the displacement parameters in this manner did not substantially degrade the quality of fit as indicated by the minor increase in the fit parameters obtained using positive displacement parameters, $R_{wp} = 6.46$, $\chi^2 = 2.60$. The final structural refinements for Ba_2NdMoO_6 refined the displacement parameters in order to provide a full estimate of the errors in the interatomic distances. However, we note that although the negative displacement parameters are indicative of imperfect data, the values lie within a few standard deviations of physically meaningful, positive values.

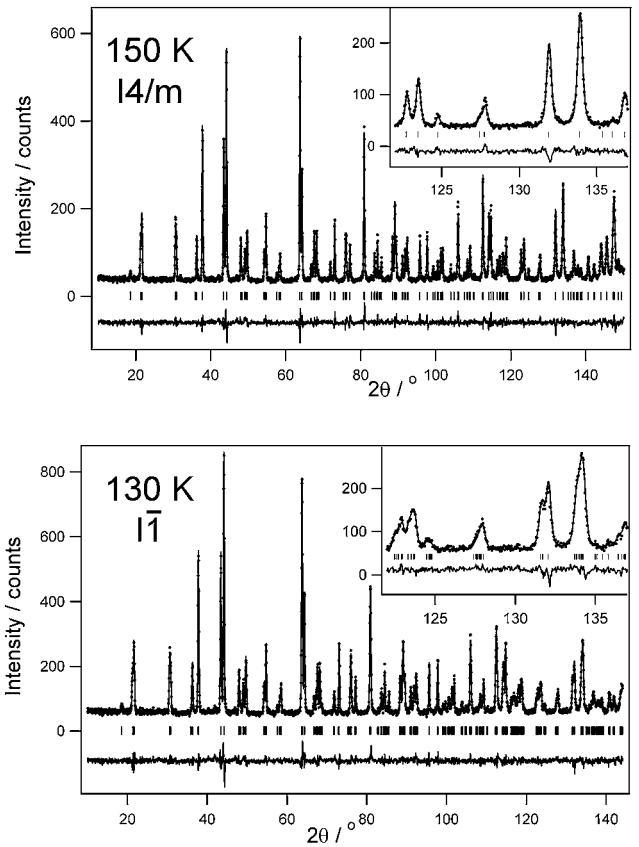

Fig. 2 Fitted neutron diffraction profiles collected at (a) 150 K and (b) 130 K. The structural transition between these two temperatures is evident from the peak splitting at low d-spacings shown in detail in the insets. Observed data are shown as dots, the calculated profile and difference are represented as lines. Vertical marks indicate the positions of the crystallographically distinct Bragg reflections allowed by the space group symmetry.

Table 1 Structural information for Ba_2NdMoO_6 as a function of temperature derived from neutron powder diffraction data

	80 K $I\bar{1}$	112 K $I\bar{1}$	130 K $I\bar{1}$	150 K $I4/m$	190 K $I4/m$
a/Å	5.97083(9)	5.97345(11)	5.97625(14)	5.98555(5)	5.98819(6)
b/Å	5.9749(11)	5.9789(12)	5.9804(2)	5.98555	5.98819
c/Å	8.59974(12)	8.59898(12)	8.59650(13)	8.59510(10)	8.58260(12)
α/°	89.840(1)	89.855(2)	89.876(2)	90	90
β/°	89.907(2)	89.911(2)	89.921(3)	90	90
γ/°	89.987(2)	89.991(2)	89.994(2)	90	90
Ba x	0.000(2)	0.000(2)	−0.0002(2)	0	0
Ba y	0.4980(14)	0.499(2)	0.503(2)	1/2	1/2
Ba z	0.2493(10)	0.2489(10)	0.2468(10)	1/4	1/4
Ba $100U_{iso}$/Å^2	−0.17(4)	−0.05(4)	−0.02(5)	0.11(4)	0.11(5)
Mo/Nd U_{iso}/Å^2	−0.16(3)	−0.09(3)	−0.12(3)	−0.08(3)	−0.02(4)
O1 x	−0.0062(12)	−0.005(2)	−0.004(2)	0	0
O1 y	0.0112(8)	0.0103(9)	0.0087(13)	0	0
O1 z	0.2667(3)	0.2663(3)	0.2660(4)	0.2668(3)	0.2668(4)
O1 U_{iso}/Å^2	0.33(6)	0.47(6)	0.72(8)	0.66(5)	0.81(6)
O2 x	0.2332(7)	0.2343(10)	0.2343(10)	0.2358(3)	0.2374(3)
O2 y	0.3094(7)	0.3084(10)	0.3084(10)	0.3065(2)	0.3055(3)
O2 z	0.0004(6)	0.0012(7)	0.0012(7)	0	0
O2 $100U_{iso}$/Å^2	0.63(12)	0.47(12)	0.4(2)	0.59(3)	0.63(4)
O3 x	0.6920(7)	0.6918(8)	0.6938(10)	—	—
O3 y	0.2352(8)	0.2357(8)	0.2366(11)	—	—
O3 z	−0.0066(5)	−0.0055(5)	−0.0061(7)	—	—
O3 $100U_{iso}$/Å^2	0.37(11)	0.65(13)	0.8(2)	—	—
R_{wp}, χ^2	6.27, 2.452	6.35,2.506	7.05, 1.773	7.11,2.711	8.45, 2.024

The quality of the fit achieved for the data collected at 130 K is shown in Fig. 2 and the structural parameters and refinement details for the tetragonal and triclinic phases are presented in Table 1. Significant bond lengths and angles are listed in Table 2. The most interesting observation from these structural models is the change in the arrangement of oxide anions around the Mo^{5+} cation. These are plotted in Fig. 3 and are the only structural feature that varies substantially over this temperature range. The axes of the triclinic cell are close to orthogonal and so the a, b and c lattice parameters of these unit cells can be usefully compared to those of the tetragonal cells observed at higher temperature. Plotting these three lattice parameters as a function of temperature makes it clear that the observed variation in the unit cell dimensions is dominated by the extension in the apical Mo–O bond. As shown in Fig. 3, this bond is continuously extended on cooling Ba_2NdMoO_6 from room temperature to 140(10) K. Below this temperature no further discernible extension of the bond occurs.

The perovskite Ba_2YMoO_6 forms a cubic perovskite with the space group $Fm\bar{3}m$ and remains paramagnetic to 2 K.[19] X-Ray powder diffraction patterns collected from the most Nd-rich compounds in the series $Ba_2Nd_{1-x}Y_xMoO_6$ show the peak splitting indicative of the tetragonal distortion observed in Ba_2NdMoO_6 at room temperature. The data collected from $Ba_2Nd_{0.93}Y_{0.07}MoO_6$ are shown in Fig. 4 and the reduction in space group symmetry from cubic to tetragonal is clearly manifested in the splitting of the peaks around 70° from the single family of (620) cubic reflections to the crystallographically distinct (332), (116) and (330) reflections in the tetragonally distorted phase. These data could be fitted using the $I4/m$ space group of the Ba_2NdMoO_6 end member. However, it should be noted that the departure from the higher symmetry space group $I4/mmm$ is manifested exclusively in the oxide anion positions. Neutron diffraction studies on Ba_2NdMoO_6 have unambiguously shown that this compound adopts the distortion described in the $I4/m$ space group, but this is difficult to establish in a *prima*

Table 2 Bond lengths and angles of Ba_2NdMoO_6 as a function of temperature derived from neutron diffraction data

	80 K $I\bar{1}$	112 K $I\bar{1}$	130 K $I\bar{1}$	150 K $I4/m$	190 K $I4/m$
Mo–O(1)/Å	2.007(2) × 2	2.011(3) × 2	2.013(3) × 2	2.002(2) × 2	2.000(2) × 2
Mo–O(2)/Å	1.959(5) × 2	1.957(5) × 2	1.958(6) × 2	1.959(2) × 4	1.959(2) × 4
Mo–O(3)/Å	1.955(4) × 2	1.952(5) × 2	1.956(6) × 2	—	—
O(1)–Mo–O(2)/°	89.8(2)	89.9(2)	88.4(14)	90	90
O(1)–Mo–O(3)/°	89.6(3)	89.5(3)	89.9(6)	—	—
O(2)–Mo–O(3)/°	89.7(2)	89.9(3)	87.7(5)	—	—
Nd–O(1)/Å	2.295(2) × 2	2.291(3) × 2	2.287(3) × 2	2.293(2) × 2	2.290(3) × 2
Nd–O(2)/Å	2.315(5) × 2	2.315(5) × 2	2.316(6) × 2	2.314(2) × 4	2.317(2) × 4
Nd–O(3)/Å	2.315(4) × 2	2.319(5) × 2	2.314(6) × 2	—	—
Mo–O(1)–Nd/°	175.9(4)	176.2(4)	177.0(6)	163.77(7)	164.38(9)
Mo–O(2)–Nd/°	162.5(2)	163.1(2)	163.0(3)	180	180
Mo–O(3)–Nd/°	163.0(2)	163.2(2)	163.8(3)	—	—

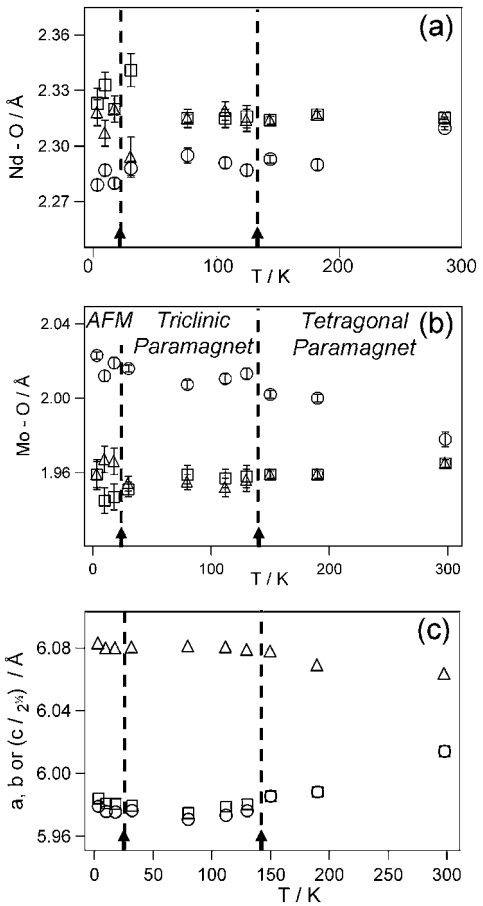

Fig. 3 The evolution in the structure of Ba_2NdMoO_6 as a function of temperature derived from neutron diffraction data. The Nd–O distances shown in (a) are invariant, within one standard deviation as shown by the error bars. The Mo–O distances illustrated in (b) show no substantial change in the Mo–O distances in the *xy* plane (shown as squares and triangles) and a significant extension of the Mo–O distance that is directed along the *z* direction (represented by circles). The leads to negative thermal expansion in the *c* lattice parameter, represented as $(c/\sqrt{2})$ by the triangles in (c) whilst the *a* and *b* lattice parameters represented by circles and squares respectively show a contraction. The estimated standard deviations in the lattice parameters are smaller than the size of the symbols. The dashed vertical lines indicate the temperature of structural and magnetic phase changes.

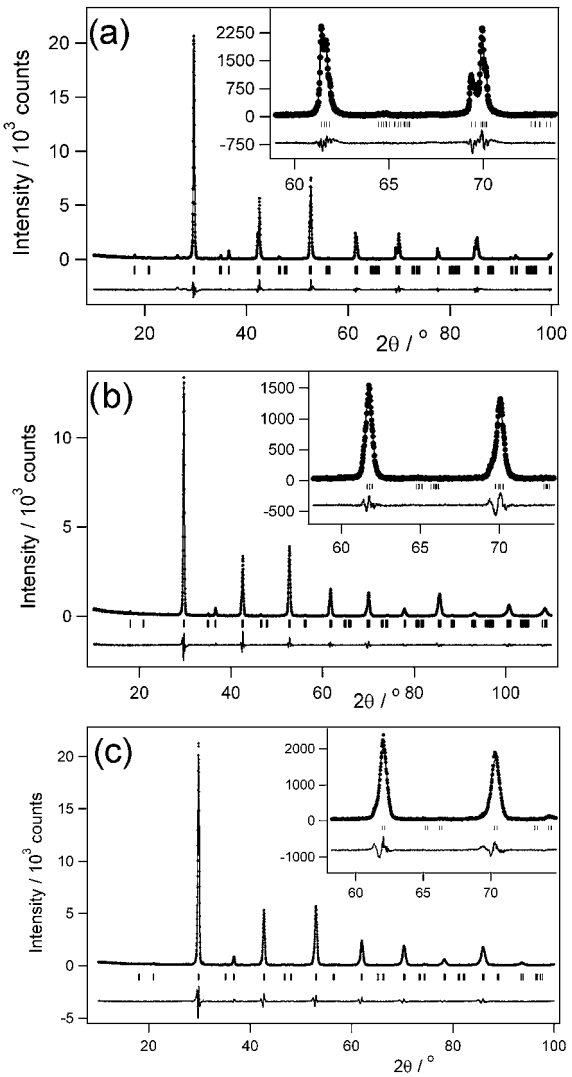

Fig. 4 X-Ray powder diffraction patterns collected from (a) $Ba_2Nd_{0.93}Y_{0.07}MoO_6$, (b) $Ba_2Nd_{0.75}Y_{0.25}MoO_6$ and (c) $Ba_2Nd_{0.50}Y_{0.50}MoO_6$. The observed data are shown as dots and the calculated diffraction profile is represented as a solid line. Vertical bars indicate the positions of allowed Bragg reflections. The inset shows the splitting of high angle peaks that is indicative of the tetragonal distortion of high Nd^{3+} contents.

facie manner from X-ray diffraction due to the dominant contribution of the scattering from the other, much heavier, elements in the compound. Hence the assignment of *I*4/*m* space group symmetry to the Nd-rich compounds in the series $Ba_2Nd_{1-x}Y_xMoO_6$ is based on the observations of the $x = 0$ composition. It is not possible to establish a precise figure for oxygen stoichiometry in these phases from the X-ray diffraction data but we note that anion vacancies have not been observed in any neutron diffraction studies[19,20] of Ba_2LnMoO_6 or $Ba_{2-x}Sr_xErMoO_6$ and so it is highly probable that oxide ion deficiency does not occur in the $BaNd_{1-x}Y_xMoO_6$ series. The consistency in the lattice parameters across this compositional series provides indirect experimental support for this conclusion.

For the compounds $x < 0.35$ the structure can be readily refined against the X-ray diffraction data to give satisfactory fits and reasonable bond lengths. For compounds $x \leq 0.35$ the peak asymmetry clearly indicated the presence of a small metric distortion from cubic symmetry and so the structure of these compositions can be assigned to the tetragonal space group *I*4/*m*. In the case of $Ba_2Nd_{0.65}Y_{0.35}MoO_6$ the model would only reach convergence if the oxide anion positions were fixed. The magnitude of the peak splitting is reduced with increasing Y^{3+} content until the data collected from a composition $Ba_2Nd_{0.5}Y_{0.5}MoO_6$ can be accurately fitted using a cubic unit cell.

Due to the shared reflection positions of these settings of the *I*4/*m* and $Fm\bar{3}m$ space groups the only indication of the structural distortion comes from the peak splitting and so for the more subtle distortions from cubic symmetry it is useful to examine the trend in lattice parameters. Fitting the data collected for compounds $x \leq 0.35$ using the tetragonal cell gives the lattice parameters shown in Fig. 5 and Table 3. The size of the distortion from cubic symmetry is progressively reduced by the

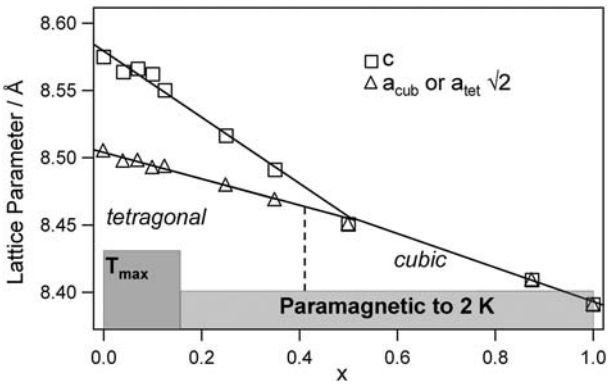

Fig. 5 The evolution in the lattice parameters of $Ba_2Nd_{1-x}Y_xMoO_6$ as a function of x derived from X-ray diffraction data collected at room temperature. In order to allow comparison between the tetragonal and face-centred cubic cells the a lattice parameter of the $I4/m$ space group is represented as $a \times \sqrt{2}$. The shaded area indicates which compositions display maxima in the magnetic susceptibility.

introduction of the smaller[25] Y^{3+} cation, $r_{Y3+} = 0.900$ Å in place of Nd^{3+}, $r_{Nd3+} = 0.983$ Å, and this leads to the elimination of the distortion for a composition in the range $0.35 < x < 0.5$. As the contribution of the oxide ions to the diffraction profile is small there are relatively large uncertainties attached to the determination of the coordinates of the anions. Nevertheless the unambiguous splitting observed for the samples containing the least Y^{3+} clearly indicates that the tetragonal distortion persists in this series Y^{3+} contents up to $Ba_2Nd_{0.65}Y_{0.35}MoO_6$.

Magnetic susceptibility measurements on $Ba_2Nd_{1-x}Y_xMoO_6$ show the temperature dependent paramagnetism associated with a fully localised electronic system. All data were fitted to the Curie–Weiss law in the range $150 < T/K < 290$ and show the negative Weiss constants indicative of the presence of antiferromagnetic interactions in this temperature range. The Weiss constants and Curie constants are collected in Table 4. The latter are compared with anticipated values which are calculated by assuming the Mo^{5+} cation displays a magnetic moment, of 1.73 μ_B, that is only due to the electronic spin whilst the Nd^{3+} cation contributes the spin–orbit coupled moment, 3.62 μ_B, due to the $^4I_{9/2}$ state of Nd^{3+}. There is no contribution from the diamagnetic Y^{3+} cation.

The compositions that are richest in Nd^{3+} show maxima in the magnetic susceptibility for $x \leq 0.125$ that are similar to the Ba_2NdMoO_6 end member of the series. The temperature of these magnetic transitions decreases slightly with magnetic dilution as the Y^{3+} content is increased but clearly shows that the magnetic ordering transition observed in Ba_2NdMoO_6 is preserved at an yttrium content of at least $Ba_2Nd_{0.875}Y_{0.125}MoO_6$ as shown in Fig. 6. Increasing the magnetic dilution further eliminates the maximum in the magnetic susceptibility and all of the more magnetically dilute phases remain paramagnetic to 2 K.

Table 3 Lattice parameters for $Ba_2Nd_{1-x}Y_xMoO_6$ determined at room temperature using X-ray powder diffraction

x	Space group	a/Å	c/Å	Vol./Å^3	R_{wp}	χ^2
0.04	$I4/m$	6.00859(9)	8.56931(14)	309.379(12)	14.01	4.90
0.07	$I4/m$	6.00899(14)	8.5661(2)	309.30(2)	15.02	5.91
0.10	$I4/m$	6.00518(13)	8.5621(2)	308.77(2)	13.47	4.29
0.125	$I4/m$	6.0058(2)	8.5502(3)	308.49(2)	12.47	2.87
0.25	$I4/m$	5.9961(2)	8.5163(5)	306.19(2)	12.59	2.92
0.35	$I4/m$	5.9960(11)	8.468(3)	304.46(3)	12.99	5.41
0.50	$Fm\bar{3}m$	8.4529(3)		603.98(6)	14.34	6.09
0.875	$Fm\bar{3}m$	8.4092(2)		594.64(3)	15.46	7.46

Table 4 Magnetic properties of the series $Ba_2Nd_{1-x}Y_xMoO_6$ derived from magnetic susceptibility measurements

x	θ/K	C/cm^3 K mol^{-1}	μ_{obs}/μ_B	μ_{calc}/μ_B[a]	T_{max}/K
0.04	−58(2)	1.79(1)	3.78(2)	3.95	15(1)
0.07	−51(1)	1.694(8)	3.68(2)	3.90	15(1)
0.10	−51(2)	1.72(1)	3.71(2)	3.85	10(1)
0.125	−53(2)	1.65(1)	3.63(2)	3.80	12(1)
0.25	−52(2)	1.55(1)	3.52(2)	3.58	—
0.35	−52(2)	1.267(9)	3.18(2)	3.39	—
0.5	−69(2)	1.145(7)	3.02(2)	3.09	—
0.875	−116(5)	0.487(8)	1.97(2)	2.15	—

[a] μ_{calc} was determined by assuming the spin-only contribution from Mo^{5+} and the full spin-orbit coupled moment from Nd^{3+} *i.e.* $\mu_{calc} = ([g(1/2(1/2 = 1))]^{1/2} + (1 - x)[g(J(J + 1))^{1/2}])$.

Discussion

Our previous structural study of Ba_2NdMoO_6 showed that this compound adopts a cation-ordered perovskite structure with a strict alternation of Nd^{3+} and Mo^{5+} over the six-coordinate sites of the structure. At room temperature the structure adopts a tetragonally distorted structure with largely regular MoO_6 octahedra. The variable temperature neutron diffraction data presented in this paper show that on cooling below room temperature the MoO_6 units distort with an elongation of the apical Mo–O distance whilst the equatorial oxide anions remain at a largely constant distance from the Mo^{5+} cation. The elongation in the bond increases progressively down to 150 K without breaking the constraints of the $I4/m$ space group symmetry. Between 130 and 150 K this Mo–O distance increases further and a structural transition to a triclinically distorted phase occurs. Once this phase change has taken place the distortion of the MoO_6 remains constant on cooling to 3.5 K. The NdO_6 octahedra that are ordered in a rock salt array with the MoO_6 units remain largely regular and show a small compression in the bond between Nd and the oxide that is displaced away from the adjacent Mo^{5+} cation. Consequently the distortion of the MoO_6 units is largely mirrored in the lattice parameters of the unit cell. It is particularly noteworthy that there are no significant structural adjustments in the vicinity of the Néel temperature of 15 K.

These observations in Ba_2NdMoO_6 provide substantial differences from those of Ba_2SmMoO_6, hitherto the only other Mo^{5+} compound reported to show a Jahn–Teller distortion. In Ba_2SmMoO_6 the compound undergoes a similar reduction in symmetry from $I4/m$ to $I\bar{1}$ but at a much higher temperature of 353 K. Crucially the MoO_6 units in Ba_2SmMoO_6 remain largely regular during the transition indicating that the Jahn–Teller distortion is not the key driver for this phase change. Instead, the MoO_6 octahedra undergo a pseudo-tetragonal elongation at the Néel temperature of 130 K. Thus it has been suggested that in Ba_2SmMoO_6 the orbital ordering resulting from the Jahn–Teller distortion precipitates long range antiferromagnetism. Our

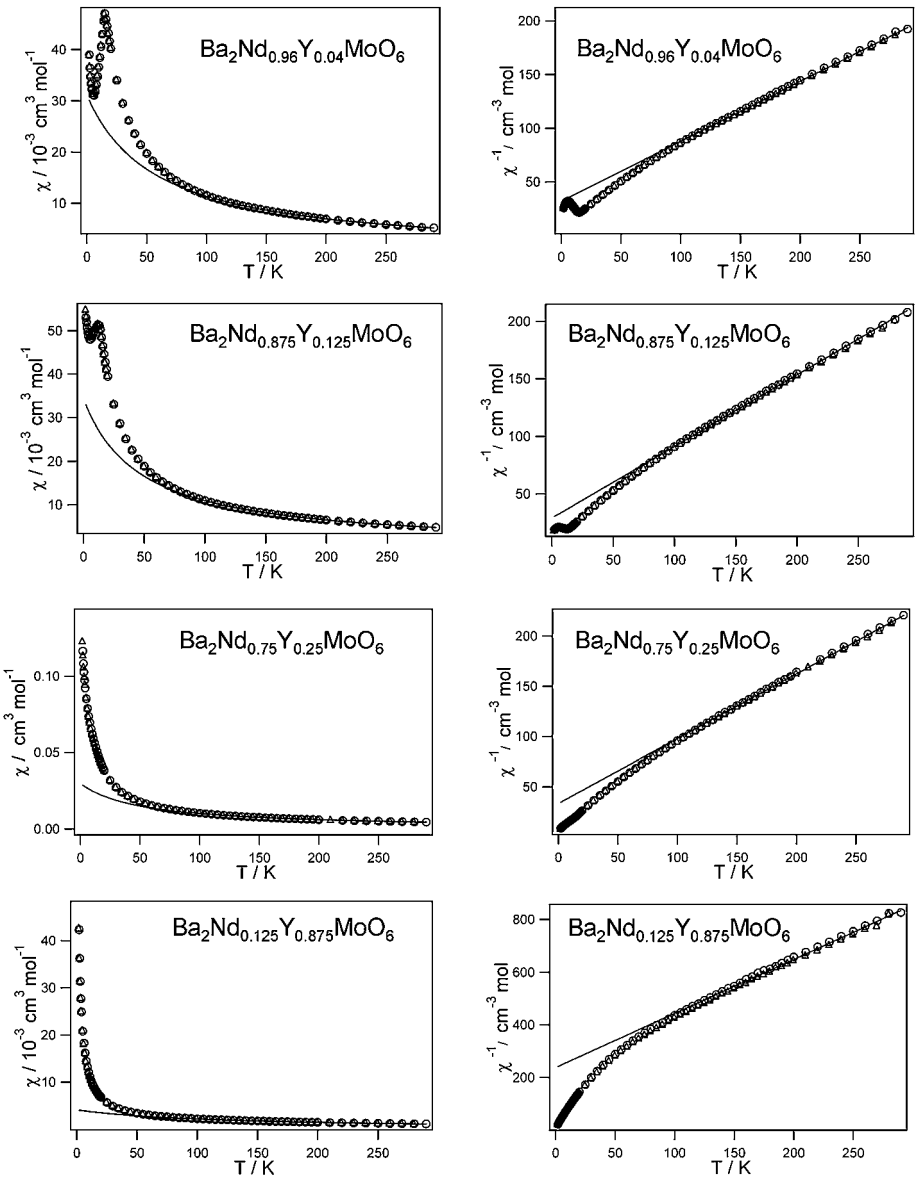

Fig. 6 The magnetic susceptibilities of selected compositions from the series $Ba_2Nd_{1-x}Y_xMoO_6$ collected after cooling the sample in zero applied field (circles) or the measuring field of 100 G (triangles). Data collected above 150 K were fitted to the Curie–Weiss law as indicated by a solid line.

observations of Ba_2NdMoO_6 show a structural phase change, magnetic ordering and an evolving Jahn–Teller distortion of the MoO_6 occurring at different temperatures. The magnitude of the Jahn–Teller distortion is similar in both compounds, once it is fully expressed, and occurs at a similar temperature, around 130 K, in both compounds. However, it is a striking difference that in the case of Ba_2NdMoO_6 the distortion evolves continuously over a temperature range of at least 70 K, whereas in the case of Ba_2SmMoO_6 the distortion reaches a maximum value over a range of no more than 20 K and may actually occur at a single temperature.

It has been suggested that there is a strong correlation between magnetic order and the structural Jahn–Teller distortion in Ba_2SmMoO_6. The behaviour of Ba_2NdMoO_6 suggests considerably weaker correlation in this compound and it may be that the correlation between the structural and electronic behaviour is stronger in Ba_2SmMoO_6 than in Ba_2NdMoO_6. Such a situation would explain the higher Néel temperature in Ba_2SmMoO_6 and it may be that this magnetic ordering provides additional stabilisation for the Jahn–Teller distortion and thus precipitation of magnetic order leads to a elongation in MoO_6 octahedra occurring at a single, discrete temperature as opposed to the continuous, progressive temperature dependence observed in Ba_2NdMoO_6.

In order to examine the magnetic ordering behaviour further we have looked at the effect of magnetic dilution and reducing the magnitude of the structural distortion by introducing the smaller, diamagnetic Y^{3+} cation into Ba_2NdMoO_6. We have previously established that the frustration inherent in the face-centred array of magnetic cations that results from the cation ordering in the cubic perovskites Ba_2LnMoO_6 (*Ln* is Gd–Yb) prevents magnetic ordering down to 2 K. Studies of the distorted phases $Ba_{2-x}Sr_xErMoO_6$ have shown that even when a substantial monoclinic distortion lifts the frustration, the Néel

temperature reaches a maximum of only 4(1) K in the heavily distorted phase Sr_2ErMoO_6.[20] Thus where the relatively modest tetragonal distortion, as observed at room temperature in Ba_2NdMoO_6, is associated with magnetic transitions significantly higher than 4 K it can be interpreted as a signature of Jahn–Teller distortion of the MoO_6 octahedra.

The structure of the compounds in the series $Ba_2Nd_{1-x}Y_xMoO_6$ follows the anticipated trend; the magnitude of the tetragonal distortion from cubic symmetry is progressively reduced with increasing Y^{3+} content. This can readily be rationalised by considering the relative sizes of the cations; consideration of the tolerance factors of Ba_2NdMoO_6 and Ba_2YMoO_6 shows that no distortion is necessary in the latter to provide reasonable bonding environments for all three cations. Diffraction experiments provide a structural model that is averaged across multiple unit cells and so application of bond valence sums to compounds such as $Ba_2Nd_{1-x}Y_xMoO_6$ that contain cation disorder is not likely to yield meaningful parameters. Moreover, the dominance of the X-ray diffraction profile by the relatively heavy cations means that considerable uncertainty is attached to the oxide anion positions. However, the trend in lattice parameters is unambiguous and shows that the transition from tetragonally distorted perovskite to ideal face-centred cubic structure occurs at a composition in the range $0.35 < x < 0.5$.

The magnetic behaviour of these compounds at high temperature can be largely understood with reference to the Curie–Weiss law, demonstrating that the electrons remain highly localised on the individual cations. In all compositions there are substantial antiferromagnetic interactions that could lead to magnetic ordering at temperatures *ca.* 50 K but competing super-exchange interactions frustrate the formation of a magnetically ordered state at these temperatures. However, for $x \leq 0.125$ a maximum is observed in the magnetic susceptibility at $T > 10$ K indicating that the frustration has been significantly lifted. The relatively high value of this magnetic ordering temperature, when compared to $T_N \leq 3.5$ K for heavily distorted compounds in the $Ba_{2-x}Sr_xErMoO_6$ system, suggests that the maxima observed in $Ba_2Nd_{1-x}Y_xMoO_6$ are indicative of a similar Jahn–Teller distortion of the MoO_6 to that observed in Ba_2NdMoO_6. It is also interesting to note that the maximum in the magnetic susceptibility does not scale with the magnitude in the tetragonal distortion; the ordering temperature is largely constant for $x \leq 0.125$ but for $0.125 < x \leq 0.25$ the samples remain paramagnetic to 2 K despite the presence of a tetragonal distortion at room temperature. These observations show for the first time that the anomalous magnetic transition temperature associated with the Jahn–Teller activity of molybdates can survive cation disorder and suggests that these molybdates are susceptible to further structural manipulation *via* chemical doping.

Acknowledgements

We wish to thank the Royal Society for the provision of a University Research Fellowship to EJC and to the University of Strathclyde for funding. We are grateful to the Institut Laue Langevin for beamtime and to Dr Paul Henry for assistance with neutron scattering experiments.

References

1 R. H. Mitchell, *Perovskites: Modern and Ancient*, Almaz Press, Thunder Bay, Ontario, 2002.
2 V. M. Goldschmidt, *Mat.-Naturv. Kl.*, 1926, **2**, 117.
3 A. M. Glazer, *Acta Crystallogr., Sect. B: Struct. Crystallogr. Cryst. Chem.*, 1972, **28**, 3384.
4 D. L. Novikov, A. J. Freeman, K. R. Poeppelmeier and V. P. Zhukov, *Physica C (Amsterdam)*, 1995, **252**, 7.
5 S. Mori, C. H. Chen and S. W. Cheong, *Nature*, 1998, **392**, 473.
6 S. Byeon, S.-S. Lee, J. B. Parise, P. M. Woodward and N. H. Hur, *Chem. Mater.*, 2005, **17**, 3552.
7 K.-I. Kobayashi, T. Kimura, H. Sawada, K. Terakura and Y. Tokura, *Nature*, 1998, **395**, 677.
8 E. J. Cussen and M. F. Thomas, *J. Mater. Chem.*, 2005, **15**, 1084.
9 A. Sundaresan, R. V. K. Mangalam, A. Iyo, Y. Tanaka and C. N. R. Rao, *J. Mater. Chem.*, 2008, **18**, 2191.
10 S. J. Dunstone, J. H. Clark and M. A. Hayward, *Chem. Commun.*, 2007, 1905.
11 C. Tenailleau, M. Allix, J. B. Claridge, M. Hervieu, M. F. Thomas, J. P. Hirst and M. J. Rosseinsky, *J. Am. Chem. Soc.*, 2008, **130**, 7570.
12 A. I. Coldea, I. M. Marshall, S. J. Blundell, J. Singleton, L. D. Noailles, P. D. Battle and M. J. Rosseinsky, *Phys. Rev. B: Condens. Matter*, 2000, **62**, R6077.
13 M. Yashima, M. Itoh, Y. Inaguma and Y. Morii, *J. Am. Chem. Soc.*, 2005, **127**, 3491.
14 T. Choi, S. Lee, Y. J. Choi, V. Kiryukhin and S.-W. Cheong, *Science*, 2008, **324**, 63.
15 C. Ritter, M. R. Ibarra, L. Morellon, J. Blasco, J. Garcia and J. M. De Teresa, *J. Phys.: Condens. Matter*, 2000, **12**, 8295.
16 C. J. Howard, B. J. Kennedy and P. M. Woodward, *Acta Crystallogr., Sect. B: Struct. Sci.*, 2003, **59**, 463.
17 A. Harrison, *J. Phys.: Condens. Matter*, 2004, **16**, S553.
18 A. C. Mclaughlin, *Solid State Commun.*, 2006, **137**, 354.
19 E. J. Cussen, D. R. Lynham and J. Rogers, *Chem. Mater.*, 2006, **18**, 2855.
20 E. J. Cussen, *J. Solid State Chem.*, 2007, **180**, 474.
21 A. C. Mclaughlin, *Phys. Rev. B: Condens. Matter*, 2008, **78**, 132404.
22 H. M. Rietveld, *J. Appl. Crystallogr.*, 1969, **2**, 65.
23 A. C. Larson and R. B. von Dreele, *General Structure Analysis System (GSAS)*, Los Alamos National Laboratories, Los Alamos, NM, 1990.
24 R. J. Hill and H. D. Flack, *J. Appl. Crystallogr.*, 1987, **20**, 356.
25 R. D. Shannon, *Acta Crystallogr., Sect. A: Cryst. Phys., Diffr., Theor. Gen. Cryst.*, 1976, **32**, 751.